ELSEVIER

Engineering Analysis with Boundary Elements 29 (2005) 1000–1007

ENGINEERING ANALYSIS *with* BOUNDARY ELEMENTS

www.elsevier.com/locate/enganabound

BEM modeling of damping forces on MEMS with thin plates

Subrata Mukherjee [a,*], Srinivas Telukunta [b], Yu Xie Mukherjee [c]

[a] *Department of Theoretical and Applied Mechanics, Cornell University, Kimball Hall, Ithaca, NY 14853, USA*
[b] *Sibley School of Mechanical and Aerospace Engineering, Kimball Hall, Cornell University, Ithaca, NY 14853, USA*
[c] *Avant Analysis Technology, 39 Hickory Circle, Ithaca, NY 14850, USA*

Received 31 October 2004; revised 12 May 2005; accepted 17 May 2005
Available online 10 October 2005

Abstract

An incompressible fluid Stokes flow model is often useful for the determination of damping forces on Micro-Electro-Mechanical (MEM) structures. Such structures in the shape of thin beams and plates are of primary interest in this work. Two difficulties arise with the standard Boundary Element Method (BEM) analysis of this problem. The first is that the usual Stokes kernel is singular; the second is numerical ill conditioning of the stiffness matrix owing to the plates being thin. A novel approach is proposed in this paper to take care of both these problems in a simple and effective manner. Sample numerical results for some simple illustrative problems are given in this paper.

Keywords: Micro-electro-mechanical systems (MEMS); Boundary element method (BEM); Thin plates; Stokes flow; Damping forces

1. Introduction

1.1. Micro-electro-mechanical systems

The field of Micro-Electro-Mechanical Systems (MEMS) is a very broad one that includes fixed or moving microstructures, encompassing micro-electro-mechanical, microfluidic, micro-opto-electro-mechanical and micro-thermo-mechanical devices and systems. MEMS usually consists of released microstructures that are suspended and anchored, or captured by a hubcap structure and set into motion by mechanical, electrical, thermal, acoustical or photonic energy source(s).

Typical MEMS structures consist of arrays of thin beams and/or plates with cross-sections in the order of micrometers (μm) and lengths in the order of tens to hundreds of micrometers. Of interest in this work is silicon MEMS, where actuation or sensing is performed electrostatically by means of arrays of capacitors. Owing to the small size of the structural elements, significant forces and/or deformations can be obtained with the application of low voltages ($\approx$10 V).

1.2. Numerical simulation of MEMS

Numerical simulation of electrically actuated MEMS devices have been carried out since the early 1990 s by using the Boundary Element Method (BEM—see, for example, [1–5]) to model the exterior electric field and the Finite Element Method (FEM—see, e.g. [6–8]) to model deformation of the structure. The commercial software package MEMCAD [9], for example, uses the commercial FEM software package ABAQUS for mechanical analysis, together with a BEM code FASTCAP [10] for the electric field analysis. Other examples of such work are [11–13]; as well as [9,14] for dynamic analysis of MEMS. Optimal shape design of MEMS has been attempted, for example, in Refs. [15–17].

1.3. MEMS with thin plates

MEMS simulations usually require BEM analysis of the electric field exterior to very thin conducting plates. A convenient way to model such a problem is to assume plates with vanishing thickness and solve for the sum of the charges on the upper and lower surfaces of each plate [18]. The standard Boundary Integral Equation (BIE) with a weakly singular kernel is used here and this approach works well for determining, for example, the capacitance of a parallel plate capacitor. For MEMS calculations, however, one must obtain the charge densities separately on the upper and lower surfaces of a plate since the traction at a surface point on a plate depends on the square of the charge density at that point. The gradient

* Corresponding author.
E-mail address: sm85@cornell.edu (S. Mukherjee).

0955-7997/$ - see front matter © 2005 Elsevier Ltd. All rights reserved.
doi:10.1016/j.enganabound.2005.05.012

BIE has been very recently employed in [19] to obtain these charge densities separately. Careful regularization of the gradient equation, to take care of singular and nearly singular integrals that arise, has been carried out in this work. Related very recent work can be found in Ref. [20]. Here, the authors have employed the dual BEM (DBEM) (i.e. the standard as well as the derivative BEM) to solve electrostatics problems involving two-dimensional (2D) parallel plate capacitors.

1.4. Damping forces on MEMS

The dynamics of MEM structures, consisting of arrays of thin plates, depends on the electrostatic field and the flow of the viscous gas surrounding the structure. An extensive literature exists on the subject of damping forces in MEMS. The key issue, of course, is the choice of a particular mathematical model in order to calculate the damping forces correctly. Various options exist, such as a squeeze film model (e.g. [21]), an incompressible steady Stokes flow model (e.g. [22]), an incompressible oscillatory Stokes flow model (e.g. [23,24]), inclusion [24] or exclusion of slip at the solid/fluid interface, or molecular dynamics (MD) simulation (e.g. [25]). The last option must be employed if continuum theory breaks down, as often happens at the nanoscale or due to extreme rarefaction of the surrounding air at very low pressures. Sometimes, even if continuum theory does apply, a quasi-steady Stokes model may not due to very high resonant frequencies (around 100 MHz [26]).

MEMS plates and beams, however, are typically tens to hundreds of micrometers long and with thickness in the order of micrometers [27]. There exists a regime where due to the micrometer-scales involved, the Reynolds numbers of the surrounding flow are generally small enough, and natural frequencies low enough (in the range of 100 s of kiloHertz) to allow the use of a steady-state Stokes flow (sometimes called creeping flow) model. Moreover, if the MEMS operate at pressures where the air can be treated as a continuum, the usual operating frequencies very often require an incompressible fluid model [22]. Further, in synthetic microjet applications, the medium surrounding the plates is typically a liquid for which an incompressible model is, of course, the appropriate one. Problems in which an incompressible steady-state Stokes model applies are of interest in this work. It is important to point out that a recent numerical and experimental study of typical MEMS structures [23] demonstrates that a 3D, incompressible, no slip, oscillatory Stokes model can predict measured quality factors within 10%. Although only the steady Stokes model is employed in the present work, it is important to note that the forms of the integral equations used here remain unchanged for the oscillatory case, provided that the appropriate kernels for oscillatory flow are used in these integral equations [23,24].

Two difficulties arise with standard BEM analysis of this problem. The first is that the usual Stokes kernel is singular; the second is numerical ill conditioning of the stiffness matrix owing to the plates being thin [22]. A novel approach is proposed here to take care of both these problems in a simple manner.

1.5. This Paper

Stokes flow for the general case is discussed first. This is followed by a discussion of Stokes flow around very thin plates. It is shown here how a Boundary Integral Equation (BIE) formulation in terms of the resultant traction overcomes problems associated with the standard BIE with the Stokes kernel. Regularized versions of the standard BIE for flow around thin flexible plates, and of the traction BIE for flow around thin rigid plates, are derived next. Some simple illustrative numerical examples involving thin flat rigid plates complete the paper.

2. Stokes flow—general case

The dynamics of MEM structures, consisting of arrays of thin plates, depends on the electrostatic field and the flow of the viscous gas surrounding the structure. Due to the micro-scales involved, the Reynolds numbers of the surrounding flow are generally small enough to allow for the use of a steady-state Stokes flow (sometimes called creeping flow) model.

The governing equations for Stokes flow are:

$$\nabla p(\mathbf{x}) - \mu \nabla^2 \mathbf{v}(\mathbf{x}) = \mathbf{0}, \quad \mathbf{x} \in B \tag{1}$$

$$\nabla \cdot \mathbf{v}(\mathbf{x}) = 0, \quad \mathbf{x} \in B \tag{2}$$

$$\mathbf{v}(\mathbf{x}) = \mathbf{g}(\mathbf{x}), \quad \mathbf{x} \in \partial B \tag{3}$$

In the above, $\mathbf{v}$ is the velocity, p is the pressure and μ is the dynamic viscosity of the fluid. Also, B is the region *exterior* to the structure and ∂B is its boundary.

The stress tensor $\boldsymbol{\sigma}$ inside the fluid, and the surface traction $\boldsymbol{\tau}$ on the solid surface, are defined by the equations

$$\boldsymbol{\sigma}(\mathbf{x}) = -p(\mathbf{x})\mathbf{I} + \mu[\nabla \mathbf{v}(\mathbf{x}) + \nabla^{\mathrm{T}} \mathbf{v}(\mathbf{x})], \quad \mathbf{x} \in B \tag{4}$$

$$\boldsymbol{\tau}(\mathbf{x}) = \boldsymbol{\sigma}(\mathbf{x}) \cdot \mathbf{n}(\mathbf{x}), \quad \mathbf{x} \in \partial B \tag{5}$$

where $\mathbf{n}$ is the unit normal to ∂B pointing into the solid.

An integral equation governing Stokes flow can be written as [28,29]

$$v_i(\mathbf{x}) = g_i(\mathbf{x}) = \oint_{\partial B} T_{ij}(\mathbf{x}, \mathbf{y}) v_j(\mathbf{y}) \mathrm{d}s(\mathbf{y}) + \int_{\partial B} G_{ij}(\mathbf{x}, \mathbf{y}) \tau_j(\mathbf{y}) \mathrm{d}s(\mathbf{y}), \quad \mathbf{x} \in \partial B \tag{6}$$

or its regularized version

$$v_i(\mathbf{x}) = g_i(\mathbf{x}) = \int_{\partial B} T_{ij}(\mathbf{x},\mathbf{y})[v_j(\mathbf{y}) - v_j(\mathbf{x})]\mathrm{d}s(\mathbf{y}) + \int_{\partial B} G_{ij}(\mathbf{x},\mathbf{y})\tau_j(\mathbf{y})\mathrm{d}s(\mathbf{y}), \quad \mathbf{x}\in\partial B \tag{7}$$

where the Green's function G is

$$G_{ij}(\mathbf{x},\mathbf{y}) = \frac{1}{8\pi\mu r}[\delta_{ij} + r_{,i}r_{,j}] \tag{8}$$

and the traction kernel is

$$T_{ij}(\mathbf{x},\mathbf{y}) = T_{ijk}(\mathbf{x},\mathbf{y})n_k(\mathbf{y}) \tag{9}$$

with:

$$T_{ijk}(\mathbf{x},\mathbf{y}) = \frac{3}{4\pi r^2} r_{,i}r_{,j}r_{,k} \tag{10}$$

In the above, $\mathbf{x}$ is a source point, $\mathbf{y}$ is a field point, r is the Euclidean distance between the source and field points, $r_{,i} = \partial r/\partial y_i = (y_i - x_i)/r$ and δ_{ij} are the components of the Kronecker delta. Also, the symbol $\oint\!\!\!\!\!\!-$ denotes the finite part of the integral in the sense of Mukherjee [30,31].

Eq. (7) follows from (6) since $\oint\!\!\!\!\!\!-_{\partial B} T_{ij}(\mathbf{x},\mathbf{y})\mathrm{d}s(\mathbf{y}) = 0$ for $\xi\in B \to \mathbf{x}\in\partial B$ (see [30,31]).

A major simplification occurs if the moving structure can be considered to be *rigid*. In this case, one gets the simple equation [28]:

$$v_i(\mathbf{x}) = g_i(\mathbf{x}) = \int_{\partial B} G_{ij}(\mathbf{x},\mathbf{y})\tau_j(\mathbf{y})\mathrm{d}s(\mathbf{y}), \quad \mathbf{x}\in\partial B \tag{11}$$

The traction vector for the rigid structure case also satisfies the higher order homogeneous equation:

$$\tau_i(\mathbf{x}) = n_k(\mathbf{x}) \oint\!\!\!\!\!\!-_{\partial B} T_{ijk}(\mathbf{x},\mathbf{y})\tau_j(\mathbf{y})\mathrm{d}s(\mathbf{y}), \quad \mathbf{x}\in\partial B \tag{12}$$

A hypersingular equation for a deformable body, which is a generalization of (12), can also be derived, but is not done in this paper. (Please see analogous derivations of BIEs for linear elastic fracture mechanics in e.g. [5]).

Eq. (11) is known to have a major 'defect'. It has a nontrivial null space of dimension N, where N is the number of conductors in the system. Each solution in the null space of $\mathbf{G}$ is of the form

$$\tau_k^{(\alpha)}(\mathbf{x}) = \begin{cases} n_k(\mathbf{x}), & \mathbf{x}\in\partial B^{(\alpha)} \\ 0, & \text{otherwise} \end{cases}, \quad \alpha = 1,2,3,\ldots N \tag{13}$$

where $\mathbf{n}(\mathbf{x})$ is the unit normal to $\partial B^{(\alpha)}$ at $\mathbf{x}$, pointing into the solid structure.

Several elegant ways of overcoming this problem have been recently suggested by Frangi and di Gioia [22]. These include use of the corresponding equations for incompressible linear elasticity, but with the Poisson's ratio ν close to the value of 0.5 (e.g. 0.499); use of a weighted linear combination of Eqs. (11) and (12), etc. These ideas are excellent for the general case. A very simple novel remedy, however, is possible for MEMS problems with very thin plates (or beams). The plate case is discussed below.

3. Stokes flow around very thin plates

3.1. Standard BIE

Analogous to the electrostatics problem [19,20] (see Fig. 1), consider the flow in a region outside of, in this case, a single thin plate. (One plate is considered for simplicity of explanation—flow around many plates can also be easily modeled.) Eq. (6), with $\mathbf{x}^+\in s^+$, is now written as

$$v_i(\mathbf{x}^+) = g_i(\mathbf{x}^+) = \oint\!\!\!\!\!\!-_{s^+} T_{ij}(\mathbf{x}^+,\mathbf{y})w_j(\mathbf{y})\mathrm{d}s(\mathbf{y}) + \int_{s^+} G_{ij}(\mathbf{x}^+,\mathbf{y})q_j(\mathbf{y})\mathrm{d}s(\mathbf{y}), \quad \mathbf{x}^+\in s^+ \tag{14}$$

where $q_j = \tau_j^+ + \tau_j^-$ and $w_j = v_j^+ - v_j^-$.

3.1.1. Rigid plate

For a rigid plate, the first integral on the right-hand side of (14) is absent (see Eq. (11)) and one gets the following simple equation:

$$v_i(\mathbf{x}^+) = g_i(\mathbf{x}^+) = \int_{s^+} G_{ij}(\mathbf{x}^+,\mathbf{y})q_j(\mathbf{y})\mathrm{d}s(\mathbf{y}), \quad \mathbf{x}^+\in s^+ \tag{15}$$

It is proved below that the null space of the kernel $\mathbf{G}$ is now empty and (15) has a unique solution for any prescribed velocity $\mathbf{g}(\mathbf{x})$ on $\partial B = s^+ \cup s^-$!

Proof 1. The homogeneous version of Eq. (11), with a single thin plate, is:

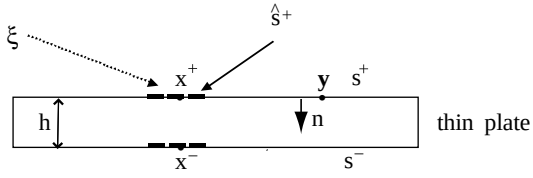

Fig. 1. A thin plate.

$$0 = \int_{\partial B} G_{ij}(\mathbf{x},\mathbf{y})\tau_j(\mathbf{y})\mathrm{d}s(\mathbf{y})$$

$$= \int_{s^+} G_{ij}(\mathbf{x},\mathbf{y})\tau_j^+(\mathbf{y})\mathrm{d}s(\mathbf{y})$$

$$+ \int_{s^-} G_{ij}(\mathbf{x},\mathbf{y})\tau_j^-(\mathbf{y})\mathrm{d}s(\mathbf{y}), \quad \mathbf{x}\in s^+\cup s^- \tag{16}$$

The only nontrivial solution of (16) is

$$\tau_j^+(\mathbf{y}) = \alpha n_j^+(\mathbf{y}), \qquad \tau_j^-(\mathbf{y}) = \alpha n_j^-(\mathbf{y}) \tag{17}$$

where α is a non-zero number. Therefore, (16) becomes:

$$0 = \int_{s^+} G_{ij}(\mathbf{x}^+,\mathbf{y})[\tau_j^+(\mathbf{y}) + \tau_j^-(\mathbf{y})]\mathrm{d}s(\mathbf{y})$$

$$= \int_{s^+} G_{ij}(\mathbf{x}^+)\alpha[n_j^+(\mathbf{y}) + n_j^-(\mathbf{y})]\mathrm{d}s(\mathbf{y})$$

$$= \int_{s^+} G_{ij}(\mathbf{x}^+,\mathbf{y})\alpha[m_j(\mathbf{y})]\mathrm{d}s(\mathbf{y}) \tag{18}$$

But $m_j = n_j^+ + n_j^- = 0$ since the normals on the two sides of the plate are equal and opposite. Therefore, the only solution of (18) is the trivial solution and the null space of the kernel in (15) is empty. □

Proof 2. Consider the equations:

$$0 = \int_{s^+} G_{ij}(\mathbf{x}^+,\mathbf{y})\tau_j(\mathbf{y})\mathrm{d}s(\mathbf{y}), \quad \mathbf{x}^+\in s^+ \tag{19}$$

$$\int_{s^+} G_{ij}(\mathbf{x}^-,\mathbf{y})\tau_j(\mathbf{y})\mathrm{d}s(\mathbf{y}) = \int_{s^+} G_{ij}(\mathbf{x}^+,\mathbf{y})\tau_j(\mathbf{y})\mathrm{d}s(\mathbf{y}),$$
$$\mathbf{x}^-\in s^-;\ \ \mathbf{x}^+\in s^+ \tag{20}$$

Please note that (20) is true within the thin plate assumption. Rewrite (19) and (20) as

$$0 = \int_{s^+\cup s^-} G_{ij}(\mathbf{x},\mathbf{y})\hat{\tau}_j\,\mathrm{d}s(\mathbf{y}), \quad \mathbf{x}\in s^+\cup s^- \tag{21}$$

where:

$$\hat{\tau}_j(\mathbf{y}) = \begin{cases} \tau_j(\mathbf{y}), & \mathbf{y}\in s^+ \\ 0, & \mathbf{y}\in s^- \end{cases} \tag{22}$$

It is known that the only solution of (21) is

$$\hat{\tau}_j(\mathbf{y}) = \alpha n_j(\mathbf{y}) \tag{23}$$

where α is a number and the unit normal (to $s^+\cup s^-$) $\mathbf{n}(\mathbf{y})\neq\mathbf{0}$, $\forall\mathbf{y}\in s^+\cup s^-$. Also, one must have the same value of α over all of $s^+\cup s^-$. Therefore, since $\alpha=0$ on s^-, it must also be zero on s^+; i.e. $\tau(\mathbf{y})=0$, $\forall\mathbf{y}\in s^+$. It follows that the only solution of (19) is:

$$\tau_j(\mathbf{y}) = 0 \tag{24}$$

In other words, the kernel $\mathbf{G}$ in Eq. (19) is invertible. □

3.1.2. Flexible plate

For a very thin flexible plate, it is possible that w_j is so small that the first integral on the right-hand side of (14) can be neglected relative to the second, so that one again ends up with Eq. (15). Otherwise, the first integral on the right-hand side of Eq. (14) can be regularized as follows (see Fig. 1):

$$\oint_{s^+} T_{ij}(\mathbf{x}^+,\mathbf{y})w_j(\mathbf{y})\mathrm{d}s(\mathbf{y})$$

$$= \int_{s^+-\hat{s}^+} T_{ij}(\mathbf{x}^+,\mathbf{y})w_j(\mathbf{y})\mathrm{d}s(\mathbf{y}) + \int_{\hat{s}^+} T_{ij}(\mathbf{x}^+,\mathbf{y})[w_j(\mathbf{y})$$

$$- w_j(\mathbf{x})]\mathrm{d}s(\mathbf{y}) + w_j(\mathbf{x})\oint_{\hat{s}^+} T_{ij}(\mathbf{x}^+,\mathbf{y})\mathrm{d}s(\mathbf{y}), \quad x^+\in\hat{s}^+ \tag{25}$$

The first term in Eq. (25) is regular, the second is weakly singular and the third is strongly singular. Using Stokes' theorem, the third term can be converted to a line integral [5]

$$\oint_{\hat{s}^+} T_{ij}(\mathbf{x}^+,\mathbf{y})\mathrm{d}s(\mathbf{y}) = g_{ij}(\mathbf{x}^+) + \frac{\Omega(\hat{s}^+,\mathbf{x}^+)}{4\pi}\delta_{ij} \tag{26}$$

where

$$g_{ij}(\mathbf{x}^+) = \frac{\varepsilon_{j\ell m}}{4\pi}\int_{\hat{\ell}^+}\frac{r_{,i}(\mathbf{x}^+,\mathbf{y})r_{,\ell}(\mathbf{x}^+,\mathbf{y})}{r(\mathbf{x}^+,\mathbf{y})}\mathrm{d}r_m \tag{27}$$

and $\Omega(\hat{s}^+,\mathbf{x}^+)$ is the solid angle subtended by $\hat{s}^+$ at the point $\mathbf{x}^+$. This is (see [19,5] and Fig. 2):

$$\Omega(\hat{s}^+,\mathbf{x}^+) = \oint_{\hat{s}^+}\frac{\mathbf{r}(\mathbf{x}^+,\mathbf{y})\cdot\mathbf{n}(\mathbf{y})}{r^3(\mathbf{x}^+,\mathbf{y})}\mathrm{d}s(\mathbf{y})$$

$$= \int_0^{2\pi}[1-\cos(\psi(\theta))]\mathrm{d}\theta \tag{28}$$

In the above, ε_{ijk} are the components of the alternating tensor, $\mathbf{r}=\mathbf{y}-\mathbf{x}$ and $r_i=y_i-x_i$.

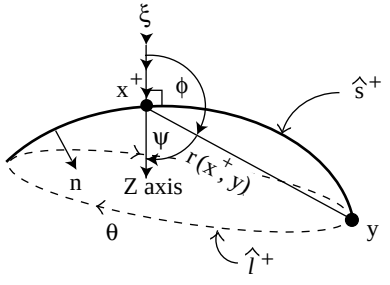

Fig. 2. Line integral for evaluation of solid angle.

In Fig. 2, a local coordinate system (x,y,z) is set up with the origin at $\mathbf{x}^+$ such that the positive z-axis intersects the surface $\hat{s}^+$. Now, ψ is the angle between the positive z-axis and $\mathbf{r}(\mathbf{x}^+,\mathbf{y})$ with $\mathbf{y}\in\hat{\ell}^+$ and θ is the angle between the positive x-axis and the projection of $\mathbf{r}(\mathbf{x}^+,\mathbf{y})$ in the xy plane. Finally, $\hat{\ell}^+$ is the bounding contour of the open surface $\hat{s}^+$.

Using Eqs. (25), (26) and (28), one finally gets a regularized version of Eq. (14) as follows:

$$
\begin{aligned}
&(1/2)[v_i(\mathbf{x}^+)+v_i(\mathbf{x}^-)]\\
&=\int_{s^+-\hat{s}^+} T_{ij}(\mathbf{x}^+,\mathbf{y})w_j(\mathbf{y})\mathrm{d}s(\mathbf{y})+\int_{\hat{s}^+} T_{ij}(\mathbf{x}^+,\mathbf{y})[w_j(\mathbf{y})\\
&\quad -w_j(\mathbf{x})]\mathrm{d}s(\mathbf{y})+g_{ij}(\mathbf{x}^+)w_j(\mathbf{x})-\frac{w_i(\mathbf{x})}{4\pi}\int_0^{2\pi}\cos\psi(\theta)\mathrm{d}\theta\\
&\quad +\int_{s^+} G_{ij}(\mathbf{x}^+,\mathbf{y})q_j(\mathbf{y})\mathrm{d}s(\mathbf{y}),\quad \mathbf{x}^+\in\hat{s}^+,\ \ \mathbf{x}^-\in\hat{s}^- \qquad (29)
\end{aligned}
$$

3.2. Traction BIE for a thin rigid plate

Usually, Eq. (29), which delivers the net traction (given the velocity), and therefore the resultant force on a plate, is sufficient for MEMS simulations. Sometimes, however, one might need to find the tractions separately. This can be done by using a thin plate version of the traction BIE.

Only the case of a thin rigid plate is considered here for the sake of simplicity. The flexible case can be considered in a manner analogous to the treatment of crack problems in linear elasticity (see, e.g. [5]).

The traction BIE (12) for a thin rigid plate can be written as (see Fig. 1):

$$
\tau_i(\mathbf{x}^+)=n_k(\mathbf{x}^+)\,\Xint=_{s^+} T_{ijk}(\mathbf{x}^+,\mathbf{y})q_j(\mathbf{y})\mathrm{d}s(\mathbf{y}),\quad \mathbf{x}^+\in s^+ \qquad (30)
$$

A regularized version of Eq. (30) is obtained as follows:

$$
\begin{aligned}
\tau_i(\mathbf{x}^+)&=n_k(\mathbf{x}^+)\int_{s^+-\hat{s}^+} T_{ijk}(\mathbf{x}^+,\mathbf{y})q_j(\mathbf{y})\mathrm{d}s(\mathbf{y})\\
&\quad +\int_{\hat{s}^+} T_{ijk}(\mathbf{x}^+,\mathbf{y})[q_j(\mathbf{y})n_k(\mathbf{x}^+)-q_j(\mathbf{x})n_k(\mathbf{y})]\mathrm{d}s(\mathbf{y})\\
&\quad +q_j(\mathbf{x})\,\Xint=_{\hat{s}^+} T_{ijk}(\mathbf{x}^+,\mathbf{y})n_k(\mathbf{y})\mathrm{d}s(\mathbf{y}),\quad \mathbf{x}^+\in\hat{s}^+ \qquad (31)
\end{aligned}
$$

The first term in Eq. (31) is regular, the second is weakly singular and the third is strongly singular. A derivation that is almost identical to that given in Section 3.1 leads to the final regularized equation:

$$
\begin{aligned}
&(1/2)[\tau_i(\mathbf{x}^+)-\tau_i(\mathbf{x}^-)]\\
&=n_k(\mathbf{x}^+)\int_{s^+-\hat{s}^+} T_{ijk}(\mathbf{x}^+,\mathbf{y})q_j(\mathbf{y})\mathrm{d}s(\mathbf{y})+\int_{\hat{s}^+} T_{ijk}(\mathbf{x}^+,\mathbf{y})\\
&\quad\times[q_j(\mathbf{y})n_k(\mathbf{x}^+)-q_j(\mathbf{x})n_k(\mathbf{y})]\mathrm{d}s(\mathbf{y})+g_{ij}(\mathbf{x}^+)q_j(\mathbf{x})\\
&\quad -\frac{q_i(\mathbf{x})}{4\pi}\int_0^{2\pi}\cos\psi(\theta)\mathrm{d}\theta,\quad \mathbf{x}^+\in\hat{s}^+,\ \ \mathbf{x}^-\in\hat{s}^- \qquad (32)
\end{aligned}
$$

Given the velocity field on the surface of a thin rigid plate, Eq. (15) can be used to solve for the sum of the tractions (i.e. the net traction) on the plate. Next, Eq. (32) can be used, *as a post-processing step*, to obtain the individual tractions, if desired, on the upper and lower surfaces of the plate.

Special case of a single thin rigid flat plate. Eqs. (15) and (32) are valid for flat as well as for curved plates (i.e. thin shells). For the case of a flat plate, however, each of the terms on the right-hand side of (32) vanishes (see below), and one is left with the simple equation:

$$
\tau_i(\mathbf{x}^+)-\tau_i(\mathbf{x}^-)=0,\quad \mathbf{x}^+\in\hat{s}^+,\ \ \mathbf{x}^-\in\hat{s}^- \qquad (33)
$$

The first term on the right-hand side of Eq. (32) vanishes since, for a flat plate, $\mathbf{r}(\mathbf{x}^+,\mathbf{y})\cdot\mathbf{n}(\mathbf{x}^+)=0$. The second term vanishes for the same reason when $r\neq 0$ and also vanishes for $r\to 0$ since it is weakly singular. Also, for a flat plate $g_{ij}(\mathbf{x}^+)=0$. This can be seen from using $\mathbf{r}(\mathbf{x}^+,\mathbf{y})\cdot\mathbf{n}(\mathbf{x}^+)=\mathbf{0}$ for $r\neq 0$ in the integrand on the left-hand side of (26) and noting that the only free term from this integral, as $r\to 0$, arises from the solid angle. Alternatively, one can directly evaluate the line integral on the right-hand side of (27), on, for example, the boundary $\hat{\ell}^+$ of a square element $\hat{s}^+$ with $\mathbf{x}^+$ being *any* point inside it, and shows that it is zero. Finally, note from Fig. 2 that $\psi=\pi/2$ for a flat plate, so that the last term on the right-hand side of (32) also vanishes.

From (33), one concludes that the traction difference $\boldsymbol{\tau}(\mathbf{x}^+)-\boldsymbol{\tau}(\mathbf{x}^-)$ vanishes on a single thin rigid flat plate of any shape!

4. Numerical results for thin rigid plate problems

4.1. Nonsingular matrix

The first example is a numerical check of the fact that the matrix $[G]$ obtained from a discretized version of Eq. (15) is, indeed, non-singular. The top surface s^+ of a flat square plate of unit side is discretized into $N\times N$ square boundary elements. The unknown function $\mathbf{q}$ is assumed to be piecewise constant on each element. (This is done purely for simplicity—linear or higher order interpolations can, of course, be easily implemented.) The condition number of the matrix $[G]$, for different levels of discretization, is shown in Table 1. It is seen that these condition numbers are small and that the matrix $[G]$ is non-singular.

Table 1
Condition number of matrix [G] (in Eq. (15)) for different levels of discretization

Discretization $N\times N$	Condition number	Condition number/N
4×4	9.78	2.445
10×10	25.40	2.540
15×15	38.30	2.553
25×25	64.02	2.561
35×35	89.32	2.552

The condition number scales approximately linearly with N.

4.2. Code verification—a circular plate moving with uniform velocity through a viscous fluid

A thin rigid flat circular plate of unit area (radius $=1/\sqrt{\pi}$) moves slowly through a viscous fluid. The plate initially lies in the x_1–x_2 plane. Two different motions are considered:

1. The velocity of the plate is $\mathbf{v}=\mathbf{k}$
2. The velocity of the plate is $\mathbf{v}=\mathbf{i}$

in consistent units. Here (**i**,**j**,**k**) are the usual Cartesian unit basis vectors. Also, the dynamic viscosity of the fluid $\mu=1$.

4.2.1. Exact and numerical solutions

This problem has an exact analytical solution for the drag on a circular plate of radius a [32]. This is $16\mu a V_0$ for $\mathbf{v}=V_0\mathbf{k}$ and $(32/3)\mu a V_0$ for $\mathbf{v}=V_0\mathbf{i}$.

Eq. (15) is solved for both cases with (a) a coarse mesh of 192 and (b) a fine mesh of 765 boundary elements on the upper plate surface s^+, with a piecewise uniform distribution of the tractions on the boundary elements. Numerical results for the drag, which is the integral of q_3 over s^+ for case 1 and of q_1 over s^+ for case 2, are shown in Table 2. Analytical results are also shown in this table. Very good agreement is observed between the numerical and analytical results.

For case 1, the distribution of the resultant traction q_3 on the plate surface s^+, obtained from the fine mesh, is shown in Fig. 3. It is seen that the resultant tractions are high near the plate edges and low everywhere else. The other resultant traction components, q_1 and q_2, are zero in this case. Similar results for case 2, again from the fine mesh, appear in Fig. 4.

4.3. A square plate moving with uniform velocity through a viscous fluid

A thin rigid flat square plate of unit side moves slowly through a viscous fluid. The plate initially lies in the x_1–x_2 plane. Two different motions are considered:

Table 2
Drag on circular plate for two different levels of discretization

Velocity	Mesh	No. of elements	Drag (numerical)	Drag (exact)	%Error
$\mathbf{v}=\mathbf{k}$	Coarse	192	−8.8669	−9.0270	1.77
$\mathbf{v}=\mathbf{k}$	Fine	765	−8.9416	−9.0270	0.95
$\mathbf{v}=\mathbf{i}$	Coarse	192	−5.9135	−6.0180	1.74
$\mathbf{v}=\mathbf{i}$	Fine	765	−5.9615	−6.0180	0.94

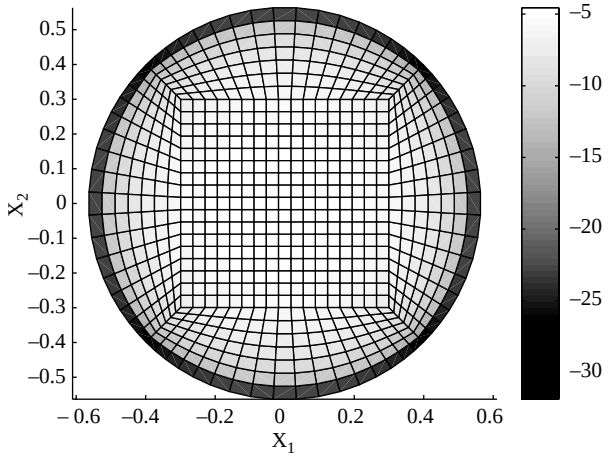

Fig. 3. Resultant traction q_3 on s^+ for $\mathbf{v}=\mathbf{k}$.

1. The velocity of the plate is $\mathbf{v}=\mathbf{k}$
2. The velocity of the plate is $\mathbf{v}=\mathbf{i}$

in consistent units. Again, the dynamic viscosity of the fluid $\mu=1$. To the best of the authors' knowledge, no analytical solution exists for this problem.

Eq. (15) is solved for both cases with 20×20 boundary elements on the upper plate surface s^+, with a piecewise uniform distribution of the tractions on the boundary elements.

4.3.1. Numerical results

Case 1. The distribution of the resultant traction q_3 on the plate surface s^+ is shown in Fig. 5. It is seen that the resultant tractions are high near the plate edges (highest at the corners) and low everywhere else. The other resultant traction components, q_1 and q_2, are zero. Combining these results with (33) leads to the conclusion:

$$\tau_3^+ = \tau_3^- = q_3/2, \qquad \tau_1^+ = \tau_1^- = 0, \qquad \tau_2^+ = \tau_2^- = 0 \tag{34}$$

Case 2. Case 2 is very similar to case 1. The distribution of the resultant traction q_1 on the plate surface s^+ is shown in Fig. 6. The other resultant traction components, q_2 and q_3, are

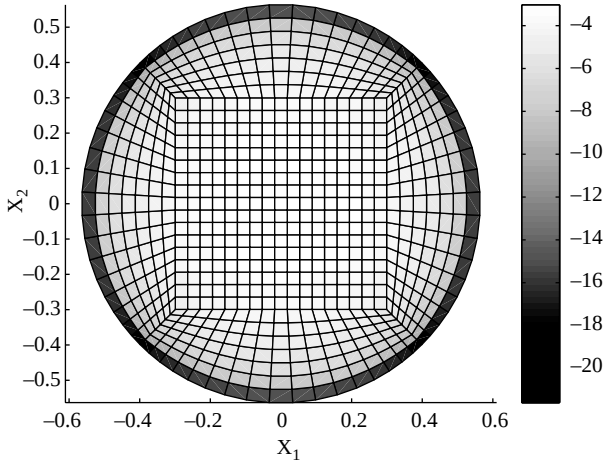

Fig. 4. Resultant traction q_1 on s^+ for $\mathbf{v}=\mathbf{i}$.

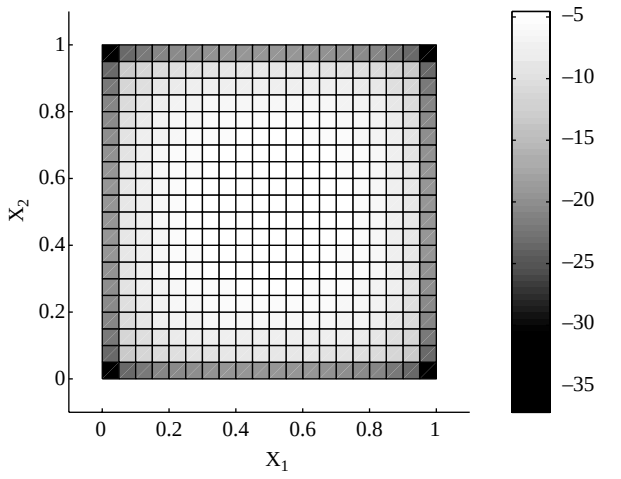

Fig. 5. Resultant traction q_3 on s^+ for $\mathbf{v}=\mathbf{k}$.

zero. Combining these results with (33) leads to the conclusion:

$$\tau_1^+ = \tau_1^- = q_1/2, \qquad \tau_2^+ = \tau_2^- = 0, \qquad \tau_3^+ = \tau_3^- = 0 \tag{35}$$

These results are analogous to the classical problem of a sphere of radius a, moving with a constant velocity $U\mathbf{e}$ (here $\mathbf{e}$ is any given unit vector) inside a viscous fluid (with dynamic viscosity μ) in Stokes flow. In this case, the (constant) traction at any point on the surface of the sphere is [33]:

$$\tau = \frac{3\mu U}{2a}\mathbf{e} \tag{36}$$

It is noted that the only non-zero traction component exists in the direction of motion and that the tractions at opposite points on the sphere surface are equal. Also, because of symmetry, the traction distribution on the sphere surface is uniform, but such is not the case for a thin plate.

Finally, it is important to mention that the traction components in Figs. 3–6, are, in fact, singular at the edges of the plate. The piecewise constant approximation for $\mathbf{q}$, of course, does not deliver these singularities—singular boundary elements must be employed for this purpose. This is a topic of continuing research.

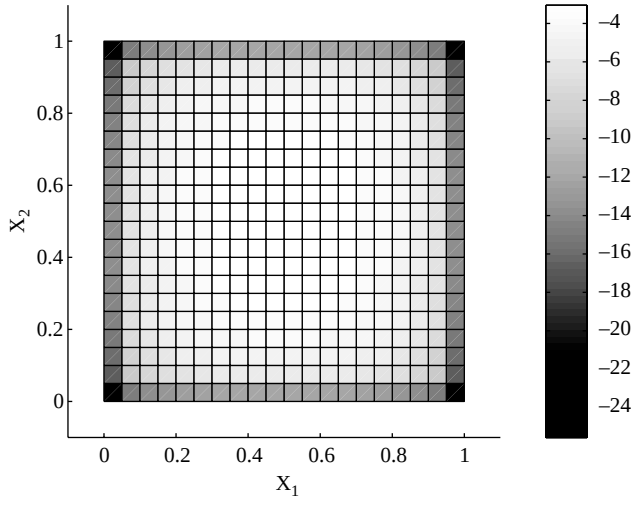

Fig. 6. Resultant traction q_1 on s^+ for $\mathbf{v}=\mathbf{i}$.

4.3.2. Mesh dependence of BEM solution

The Case 1 problem for the square plate is solved for different levels of mesh discretization. Table 3 shows computed results for $\tau_3^+(P)$ and drag for four different meshes. The coordinate axes are aligned to the edges of the (unit-sided square) plate with the origin at the left bottom corner, and the point P has coordinates (0.3,0.3). The drag, as before, is the integral of q_3 over the upper plate surface s^+. It is seen that the mesh dependence of the numerical results is minimal.

5. Concluding remarks

BEM analysis of Stokes flow around a thin plate, and calculation of the resulting forces on the plate, typically presents two challenges. The first is that the usual Stokes kernel is singular. The second arises from the fact that if flow around a very thin plate is modeled by the usual BEM, the BIEs, collocated on the upper and lower surfaces of the plate are 'nearly linearly dependent' and can lead to an ill-conditioned stiffness matrix. A novel solution to both these problems is proposed in this paper. Using ideas presented before by many researchers for the modeling of very thin cracks by the BEM (see, e.g. [5] for a discussion of this problem together with a list of references), a thin plate or shell is replaced by a mathematical surface of zero thickness. Now, the sum of the charges in an electrostatic problem [19], or the resultant traction on a plate in a Stokes flow problem, can be computed directly. If necessary, the separate charges (or tractions) can then be computed, as a post-processing step, by employing the gradient (or the traction) BIE.

A major problem, however, still remains for modeling of practical MEM structures such as comb drives or resonators. This is because the thin plates or beams in these devices are also typically packed very closely together. A scheme is presented in [19] for modeling the electrostatic problem with thin plates that are reasonably densely packed together. It has been very recently demonstrated that this idea works for electrostatic problems for parallel plates with gaps between them that are of the order of ten times a plate thickness [34]. Successful modeling of MEM structures with plates that are packed very densely together (e.g. with gaps that are of the order of a plate thickness) is still an open problem. One possible idea for solving this problem is to extrapolate BEM solutions for traction distributions as a function of gap size for gaps $\geq 10\,h$, down to gaps $\approx O(h)$. For electrostatic problems, this extrapolation scheme should be guided by the dependence of total charge density on gap (see, e.g. Fig. 8 in [19]), together with the well-known inverse square law that governs force as

Table 3
Traction component $\tau_3^+(0.3.0.3)$ and drag for different levels of discretization for $\mathbf{v}=\mathbf{k}$

Discretization $N\times N$	$\tau_3^+(0.3.0.3)$	Drag on plate
5×5	−2.5233	−8.6813
15×15	−2.6301	−9.0299
25×25	−2.6076	− 9.1041
35×35	−2.5968	−9.1364

a function of charge density. This problem is a topic of continuing research.

Acknowledgements

This research has been supported by Grant No. EEC-0303674 of the US National Science Foundation to Cornell University. The authors gratefully acknowledge this support. Any opinions, findings and conclusions or recommendations expressed in this paper are those of the authors and do not necessarily reflect the views of the National Science Foundation.

References

[1] Mukherjee S. Boundary element methods in creep and fracture. London: Applied Science Publishers; 1982.
[2] Banerjee PK. The boundary element methods in engineering. Maidenhead: McGraw Hill Europe; 1994.
[3] Chandra A, Mukherjee S. Boundary element methods in manufacturing. New York: Oxford University Press; 1997.
[4] Bonnet M. Boundary integral equation methods for solids and fluids. Chichester, UK: Wiley; 1999.
[5] Mukherjee S, Mukherjee YX. Boundary methods: elements, contours and nodes. Boca Raton, FL: Taylor and Francis/CRC Press; 2005.
[6] Yang TY. Finite element structural analysis. New Jersey: Prentice-Hall; 1986.
[7] Zienkiewicz OC, Taylor RL. The finite element method. vol. 1,2,4. Maidenhead, UK: McGraw Hill; 1994.
[8] Hughes TJR. The finite element method: linear static and dynamic finite element analysis. Mineola, NY: Dover; 2000.
[9] Senturia SD, Harris RM, Johnson BP, Kim S, Nabors K, Shulman MA, White JK. A computer-aided design system for microelectromechanical systems (MEMCAD). J Microelectromech Syst 1992;1:3–13.
[10] Nabors K, White J. FastCap: a multi-pole accelerated 3-D capacitance extraction program. IEEE Trans Comput-Aided Des 1991;10:1447–59.
[11] Gilbert JR, Legtenberg R, Senturia SD. 3D coupled electromechanics for MEMS: applications of CoSolve-EM. Proc IEEE MEMS 1995;122–7.
[12] Shi F, Ramesh P, Mukherjee S. Simulation methods for micro-electro-mechanical structures (MEMS) with application to a microtweezer. Comp Struct 1995;56:769–83.
[13] Aluru NR, White J. An efficient numerical technique for electromechanical simulation of complicated microelectromechanical structures. Sens Actuators A 1997;58:1–11.
[14] Shi F, Ramesh P, Mukherjee S. Dynamic analysis of micro-electro-mechanical systems. Int J Num Meth Eng 1996;39:4119–39.
[15] Ye W, Mukherjee S, MacDonald NC. Optimal shape design of an electrostatic comb drive in micro-electro-mechanical systems. J Microelectromech Syst 1998;7:16–26.
[16] Ye W, Mukherjee S. Optimal shape design of three-dimensional MEMS with applications to electrostatic comb drives. Int J Num Meth Eng 1999; 45:175–94.
[17] Ye W, Mukherjee S. Design and fabrication of an electrostatic variable gap drive in micro-electro-mechanical systems. Comp Mod Eng Sci 2000; 1:111–20.
[18] Harrington RF. Field computation by moment methods. Piscataway, NJ: IEEE Press; 1993.
[19] Bao Z, Mukherjee S, Electrostatic BEM, for MEMS. with thin conducting plates and shells. Eng Anal Boundary Elements 2004;28:1427–35.
[20] Liao Y-S, Chyuan S-W, Chen J-T. Efficaciously modeling exterior electrostatic problems with singularity for electron devices. IEEE Circuits Devices Mag 2004;25–34.
[21] Pan F, Kubby J, Peeters E, Tran AT, Mukherjee S. Squeeze film damping effect on the dynamic response of a MEMS torsion mirror. J Micromech Microeng 1998;8:200–8.
[22] Frangi A, di Gioia A. Multipole BEM for the evaluation of damping forces on MEMS. Comput Mech [In press].
[23] Ye W, Wang X, Hemmert W, Freeman D, White J. Air damping in laterally oscillating microresonators: a numerical and experimental study. J Microelectromech Syst 2003;12:557–66.
[24] Ding J, Ye W. A fast integral approach for drag force calculation due to oscillatory slip Stokes flows. Int J Num Meth Eng 2004;60:1535–67.
[25] Hutcherson S, Ye W. On the squeeze film damping of micro-resonators in the free-molecule regime. J Micromech Microeng 2004;14:1726–33.
[26] Bhiladvala RB, Wang ZJ. Effect of fluids on the Q factor and resonance frequency of oscillating micrometer and nanometer scale beams. Phys Rev E 2004;69:036307.
[27] Bao Z, Mukherjee S, Roman M, Aubry N. Nonlinear vibrations of beams, strings, plates and membranes without initial tension. ASME J Appl Mech 2004;71:551–9.
[28] Pozrikidis C. Boundary integral and singularity methods for linearized viscous flow. Cambridge, UK: Cambridge University Press; 1992.
[29] Sladek V. Private communication. 2004.
[30] Mukherjee S. CPV and HFP integrals and their applications in the boundary element method. Int J Solids Struct 2000;37:6623–34.
[31] Mukherjee S. Finite parts of singular and hypersingular integrals with irregular boundary source points. Eng Anal Boundary Elements 2000;24: 767–76.
[32] Kanwal RP. Drag on an axially symmetric body vibrating slowly along its axis in a viscous fluid. J Fluid Mech 1964;19:631–6.
[33] Constantinescu VN. Laminar viscous flow. New York: Springer; 1995.
[34] Telukunta S, Mukherjee S. Fully Lagrangian modeling of MEMS with thin plates and shells. J Microelectromech Syst [Submitted].